Supporting Information

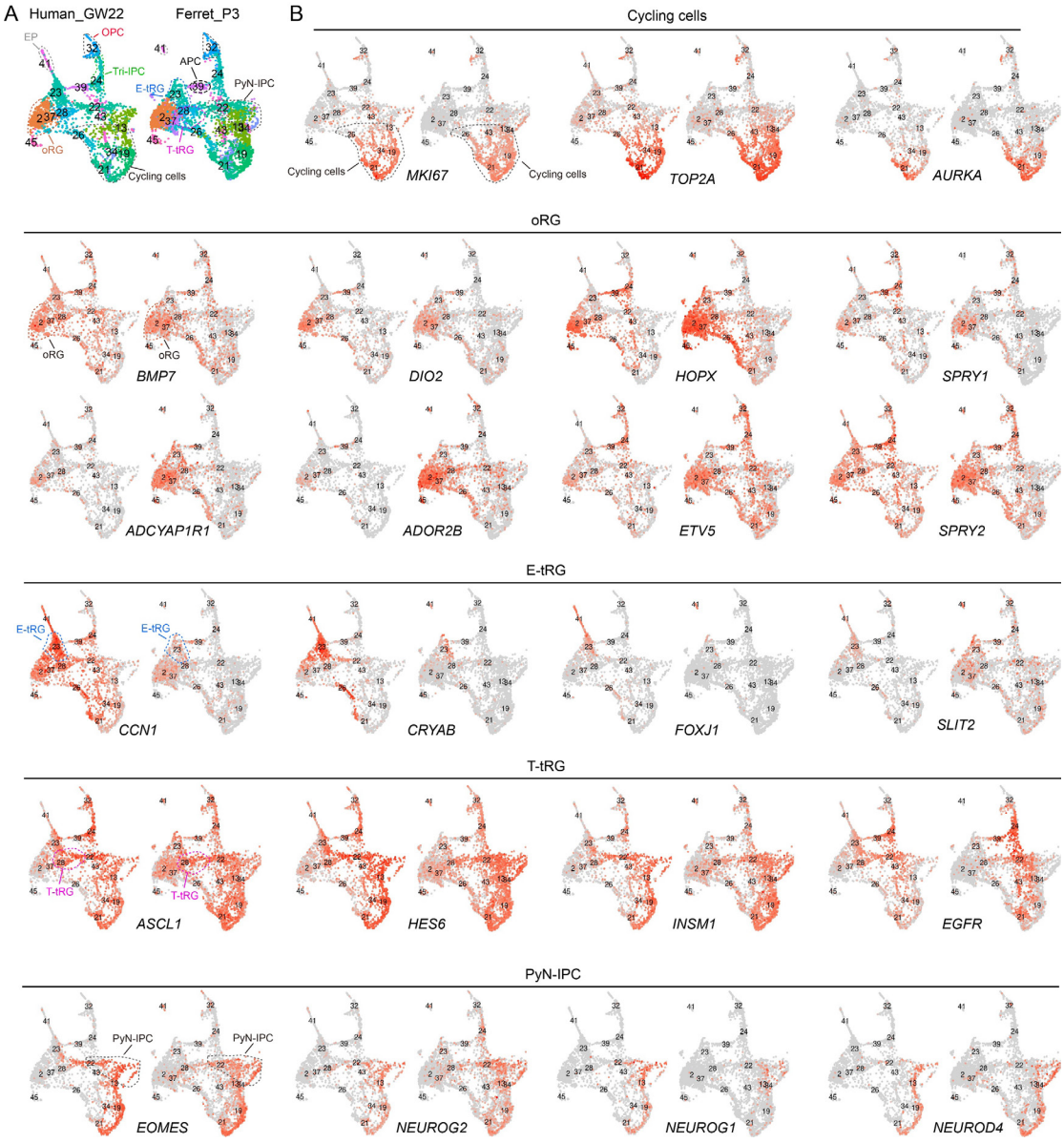

Figure S1. Expression of cell-type-specific markers in scRNA-Seq data from human GW22 and ferret P3 cortices. (A) Cluster-resolved UMAP (from Fig. 1B) showing RG and IPC populations in the human and ferret cortices. (**B)** UMAP plots showing gene expression in human and ferret cortical progenitors. Note that key components of the cortical PKA signaling, including *ADCYAP1R1, ADORA2B,* and *DIO2*, demonstrate significantly elevated expression levels in oRGs. oRG, outer radial glia; E-tRG, ependymocyte-generating truncated radial glia, T-tRG, Tri-IPC-generating tRG; PyN-IPC, PyN intermediate progenitor cells.

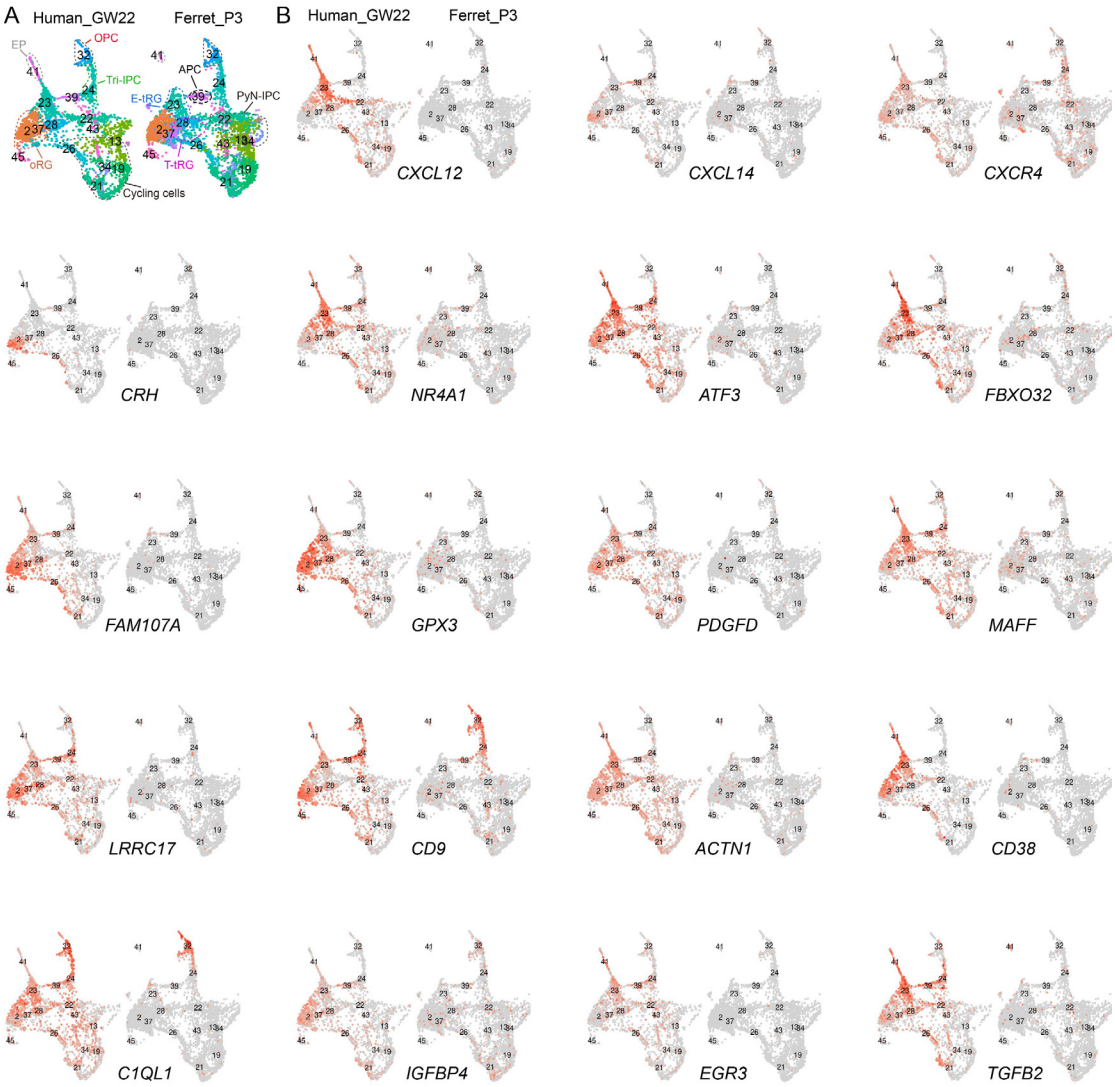

Figure S2. Divergent expression patterns of cell-type-specific markers between human (GW22) and ferret (P3) cortical RGs. (A) UMAP (from Fig. 1B) showing RG and IPC populations. (**B**) Highlighted genes exhibit robust expression in human cortical RGs but minimal or absent expression in ferret cortical RGs.

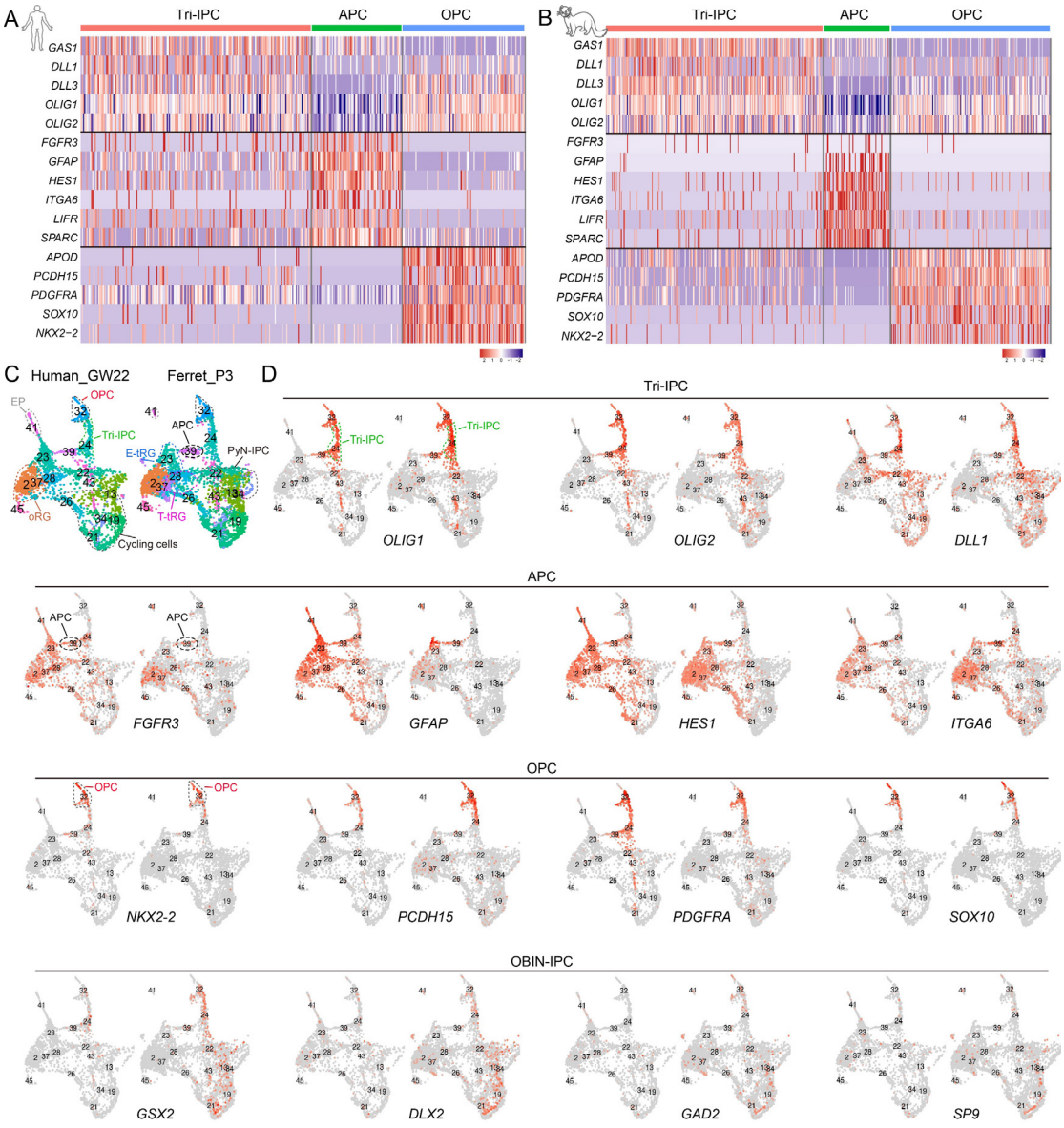

Figure S3. The molecular signatures of human and ferret cortical Tri-IPCs, APCs, and OPCs. (A, B) Heatmap of conserved gene expression in human (GW22) vs. ferret (P3) cortical Tri-IPCs, APCs, and OPCs. **(C)** UMAP (from Fig. 1B) showing cortical RG and IPC populations. (**D**) UMAP projections of gene expression in human (GW22) and ferret (P3) cortical Tri-IPCs, APCs, and OPCs reveal that the absence of a distinct OBIN-IPC cluster adjacent to Tri-IPCs suggests limited derivation of OBIN-IPCs from Tri-IPCs in both GW22 human and P3 ferret cortices. Tri-IPCs, tripotential intermediate progenitor cells; APC, astrocyte-IPCs; OPC, oligodendrocyte-IPCs; OBIN-IPC, IPCs for cortically derived olfactory bulb interneuron.

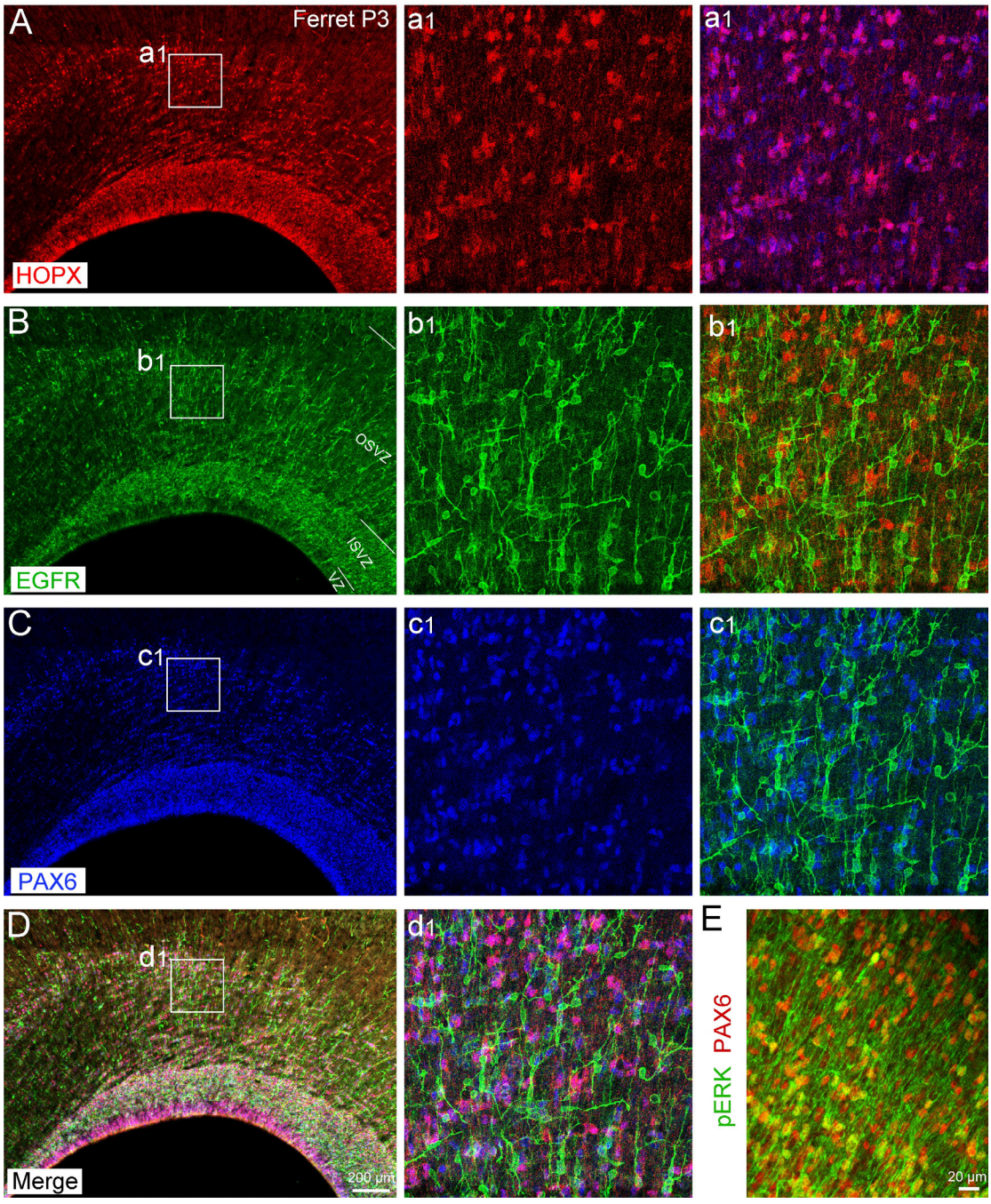

Figure S4. Ferret oRGs do not express EGFR. (**A-D)** Triple immunostaining for HOPX/PAX6/EGFR revealing that P3 ferret cortical oRGs express HOPX and PAX6, but not EGFR. **(E)** P3 cortical oRG express PAX6 and pERK.

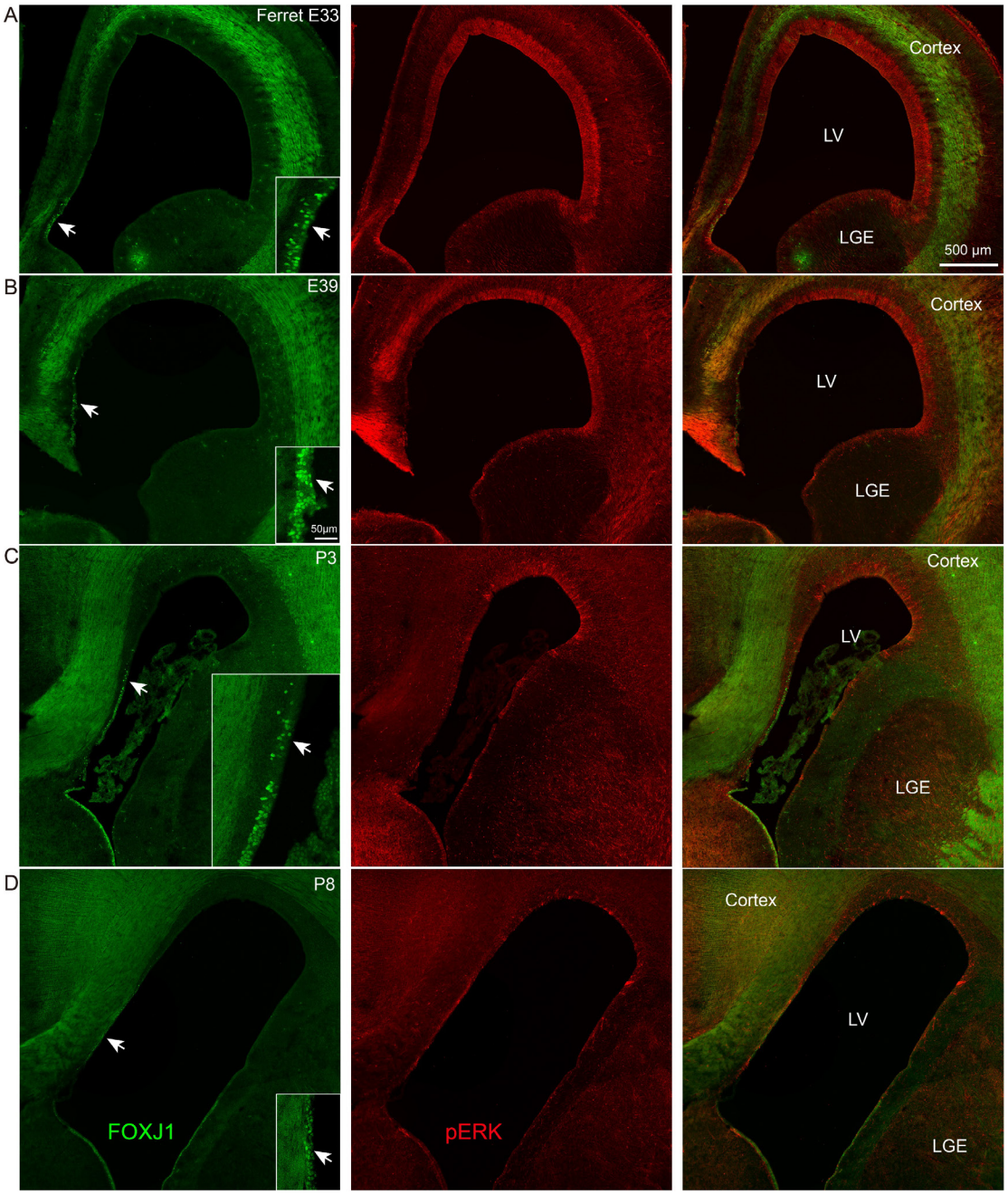

Figure S5. Spatiotemporal expansion of FOXJ1+ E-tRGs in developing ferret cortex. (A-D) FOXJ1/pERK co-staining reveals medial-to-lateral expansion of FOXJ1+ cells in cortical VZ, accompanied by a complementary medial-low to lateral-high pERK gradient (E33-P3). Note that the marked pERK reduction in lateral cortical VZ at P8 may result from both YAP and SHH signaling activation in late corticogenesis.

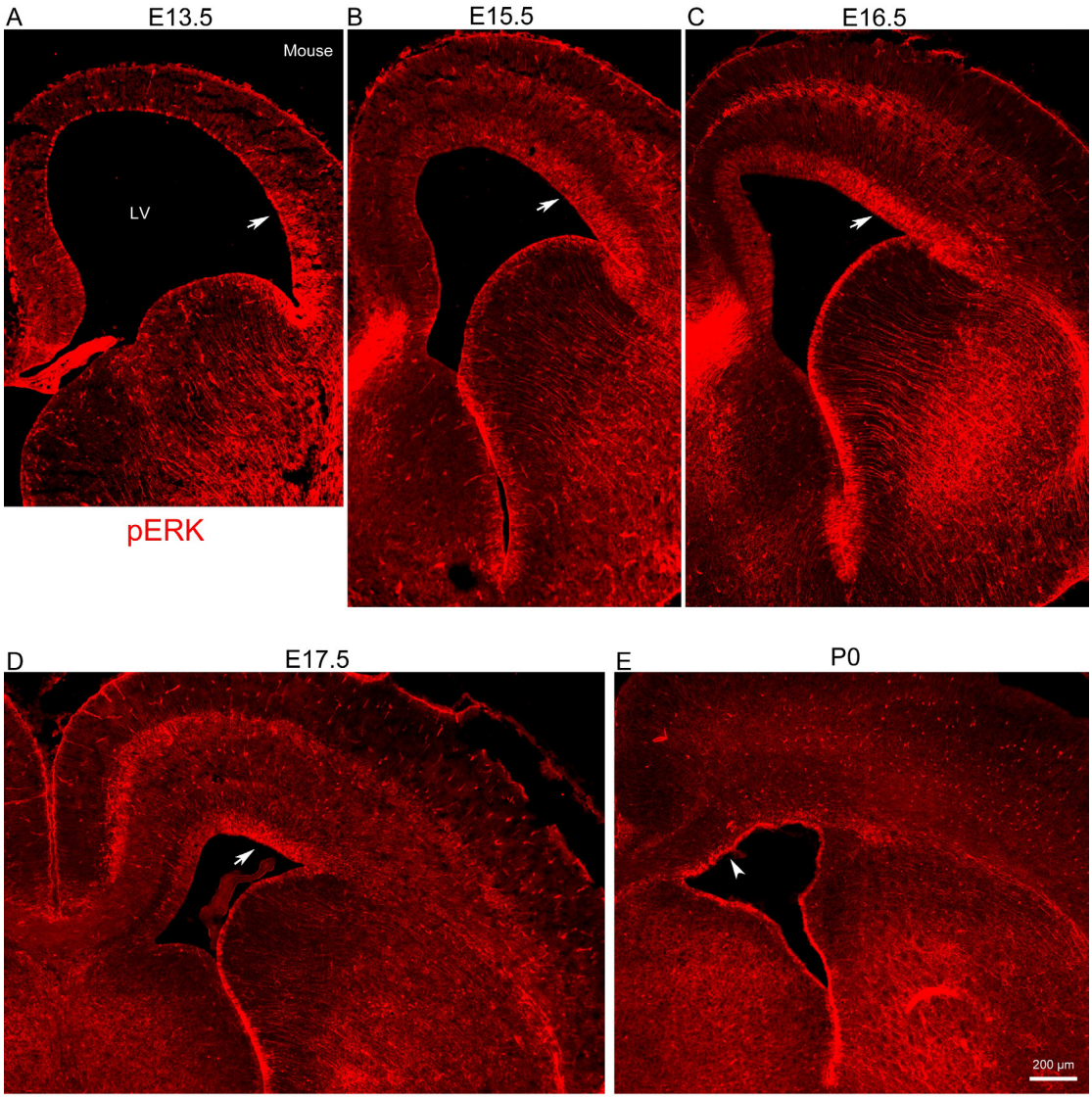

Figure S6. Spatiotemporal dynamics of pERK signaling in developing mouse cortex. (A-D) pERK immunostaining (E13.5-E17.5) demonstrates a consistent medial-low to lateral-high gradient in mouse cortical VZ. Notably, pERK expression is likely restored in medial cortical VZ by P0.

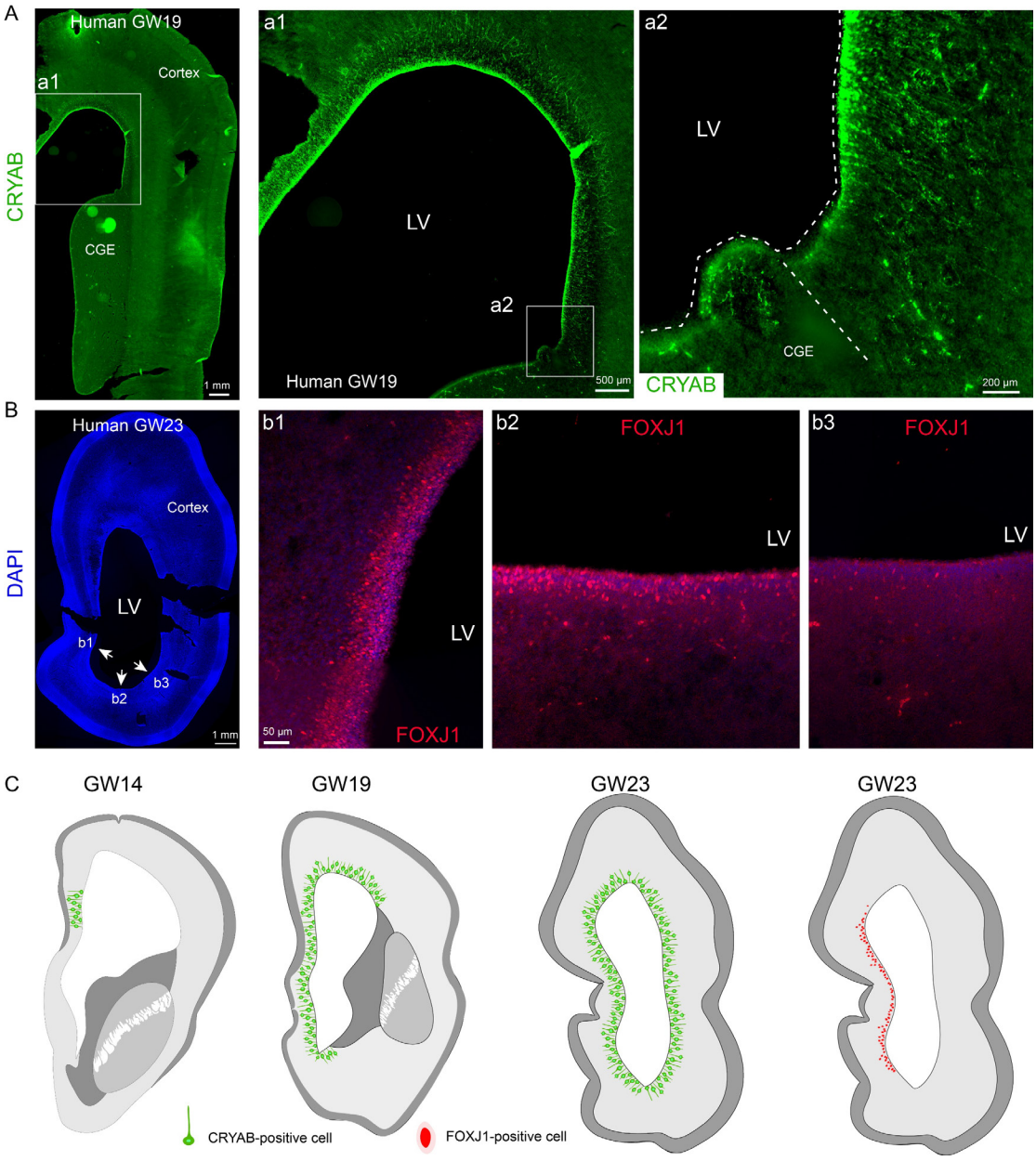

Figure S7. Spatiotemporal expression of CRYAB and FOXJ1 in developing human cortex. (A) CRYAB is specifically expressed in cortical VZ, but absent from ganglionic eminence VZ at GW19. **(B)** FOXJ1 shows medial-enriched expression in human cortical VZ at GW23. **(C)** Schematic summarizing CRYAB and FOXJ1 expression patterns across developmental stages (GW14, GW19, GW23). CGE, caudal ganglionic eminence.

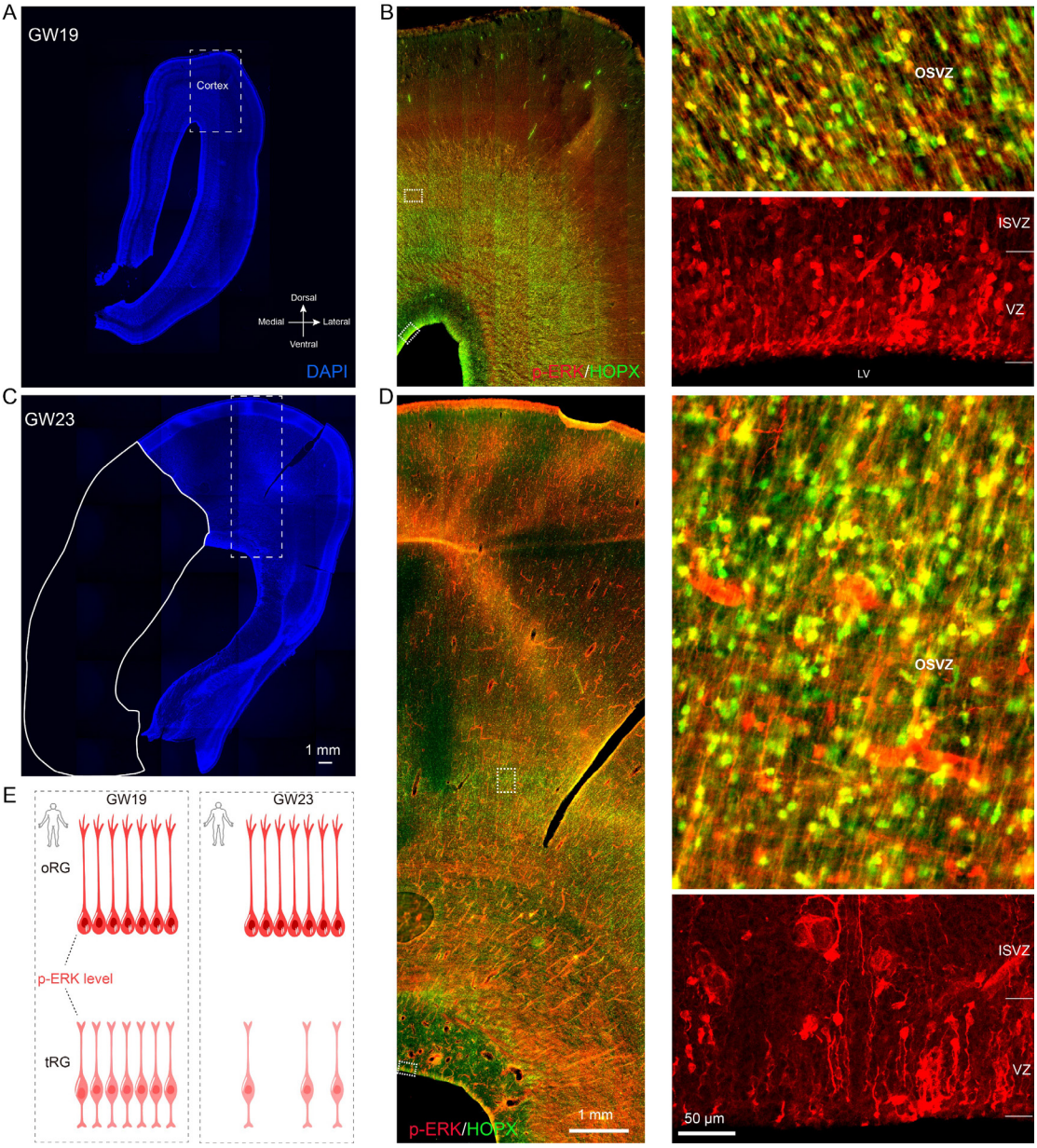

Figure S8. Developmental downregulation of ERK signaling in human cortical VZ. (A, B) At GW19, most tRGs exhibit low pERK levels in the VZ, while oRGs maintain high pERK/HOPX co-expression in the OSVZ. **(C, D)** By GW23, the population of pERK-positive tRGs shows significant reduction in the VZ, whereas oRGs persistently exhibit robust pERK and HOPX co-expression in the OSVZ. **(E)** Schematic depicting progressive ERK signaling attenuation in cortical VZ (GW19-GW23), potentially mediated by increasing YAP and SHH pathway activity.

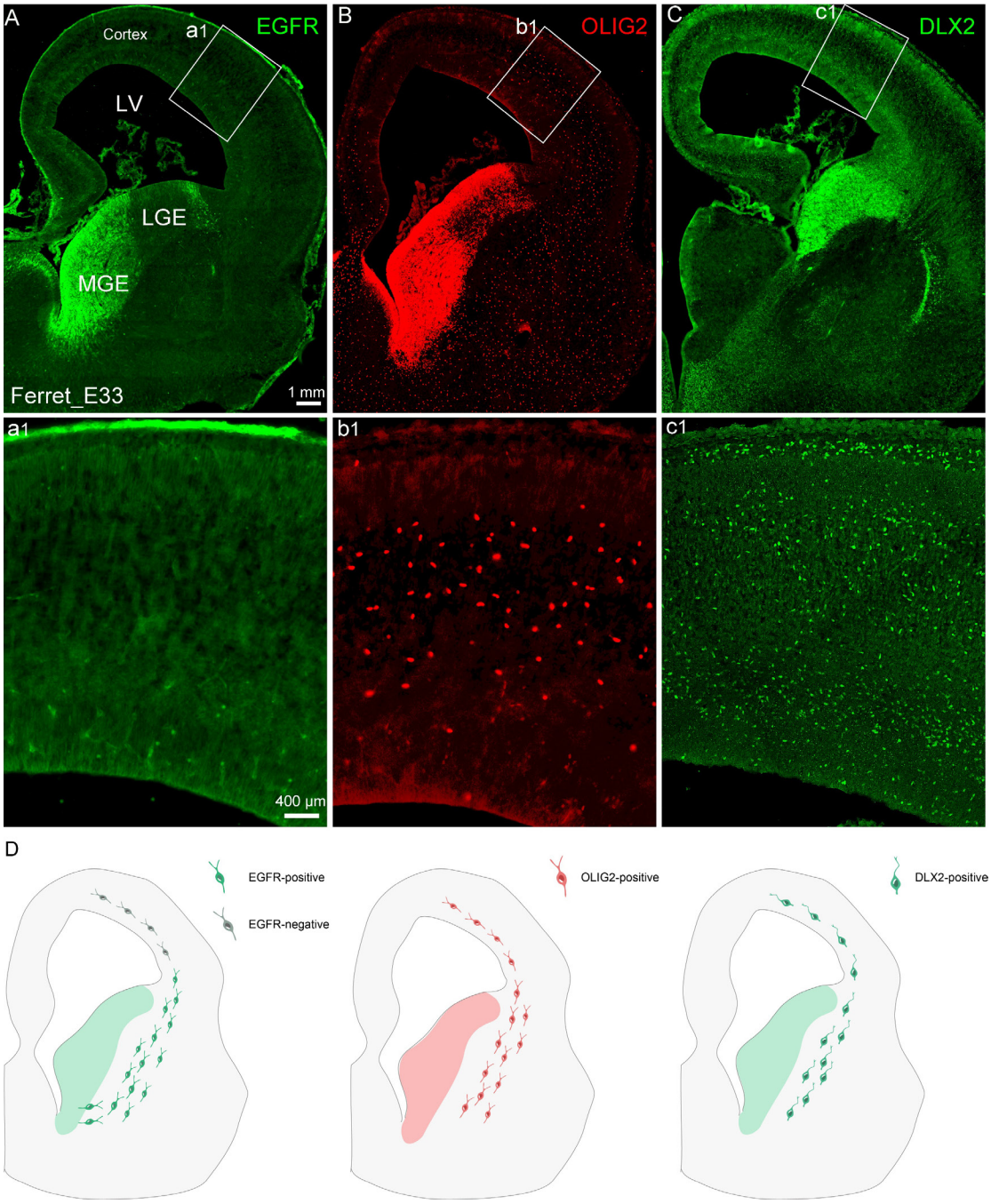

Figure S9. Ventral ganglionic eminence-derived cortical interneurons and OPCs downregulate EGFR expression upon cortical entry. (**A-C**) Coronal sections of E33 ferret brain stained for EGFR, OLIG2, and DLX2, with cortical boxed areas shown at higher magnification. (D) Schematic model demonstrating that ventral ganglionic eminence-derived cells maintain lineage markers (DLX2+ interneurons and OLIG2+ OPCs) while completely suppressing EGFR expression during cortical entry. MGE, medial ganglionic eminence.

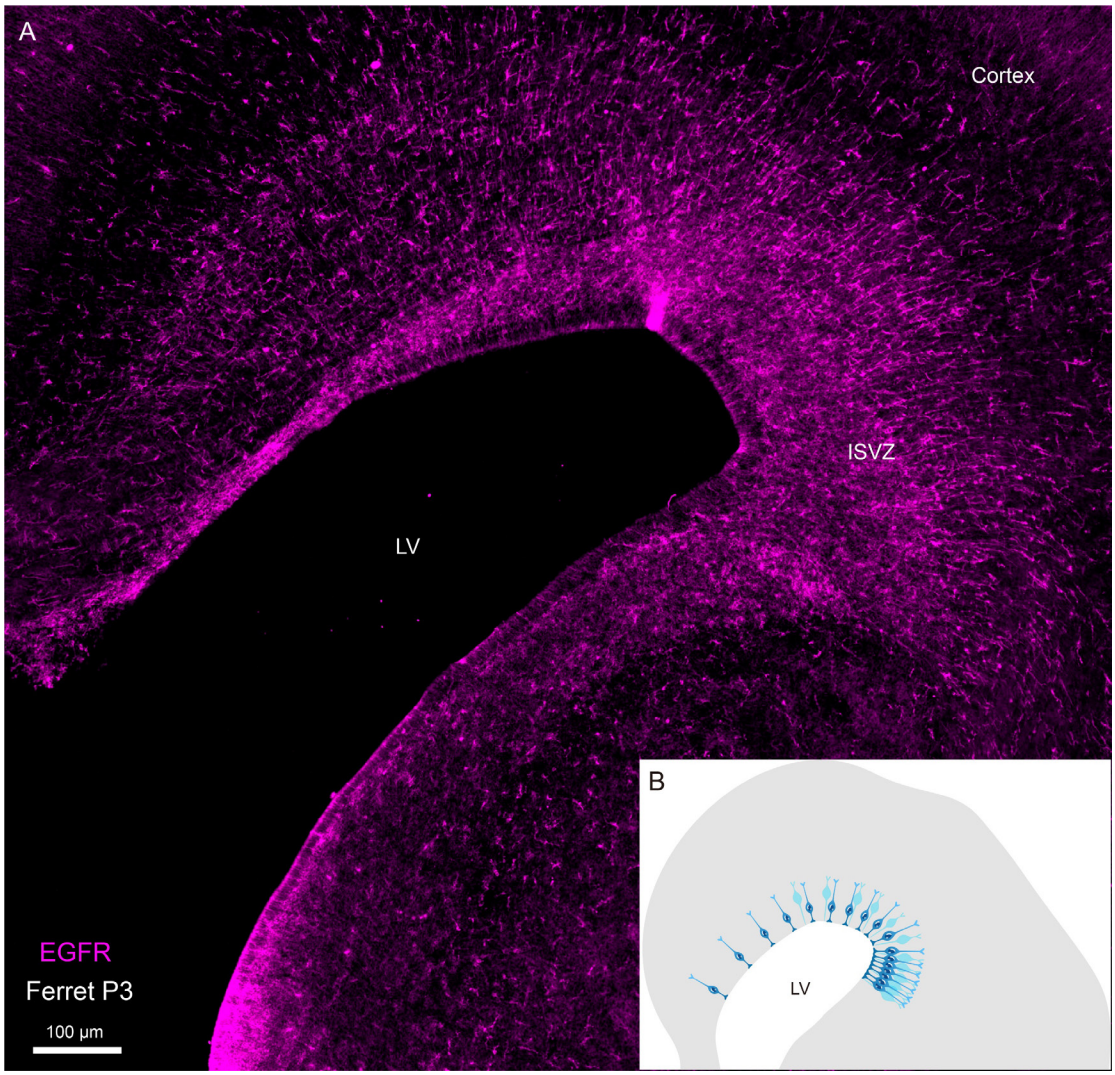

Figure S10. Mediolateral EGFR gradient in the P3 ferret cortical SVZ. (A) EGFR immunostaining in the P3 ferret cortex reveals that T-tRGs generate Tri-IPCs through lateral-to-medial progression. **(B)** Schematic model of EGFR expression patterns (medial-low to lateral-high) in neonatal ferret VZ/SVZ.

Table S1. scRNA-seq characterization of GW22 human cortex. Cluster identities: oRGs (cluster 2), E-tRGs (23), T-tRGs (28), Tri-IPCs (24), APCs (39), OPCs (32). Lists differentially expressed genes (DEGs) for: oRGs vs T-tRGs, E-tRGs vs T-tRGs, and E-tRGs vs oRGs in the GW22 human cortex.

Table S2. scRNA-seq characterization of P3 ferret cortex. Cluster identities: oRGs (cluster 2), E-tRGs (23), T-tRGs (28), Tri-IPCs (24), APCs (39), OPCs (32). Lists DEGs for: oRGs vs T-tRGs, E-tRGs vs T-tRGs, and E-tRGs vs oRGs in the P3 ferret cortex.

Table S3. Cross-species scRNA-seq analysis (human GW22 vs ferret P3 cortex). Shows DEGs between homologous populations: oRGs, E-tRGs, T-tRGs, Tri-IPCs, APCs, and OPCs.